

Quantum-enhanced Large Language Models on Quantum Hardware via Cayley Unitary Adapters

Borja Aizpurua^{1,2}, Sukhbinder Singh³, Augustine Kshetrimayum¹, Saeed S. Jahromi^{1,4}, and Román Orús^{1,4,5,*}

¹Multiverse Computing, Parque Científico y Tecnológico de Gipuzkoa, Paseo de Miramón 170, 20014, Donostia / San Sebastián, Spain

²Department of Basic Sciences, Tecnun – University of Navarra, San Sebastián, Spain

³Multiverse Computing, Centre for Social Innovation, 192 Spadina Avenue, ON M5T 2C2, Toronto, Canada

⁴Donostia International Physics Center, Paseo Manuel de Lardizabal 4, 20018, San Sebastián, Spain

⁵Ikerbasque Foundation for Science, Maria Diaz de Haro 3, 48013, Bilbao, Spain

*Correspondence: roman.orus@multiversecomputing.com

Large language models (LLMs) have transformed artificial intelligence, yet classical architectures impose a fundamental constraint: every trainable parameter demands classical memory that scales unfavourably with model size. Quantum computing offers a qualita-

tively different pathway, but practical demonstrations on real hardware have remained elusive for models of practical relevance. Here we show that Cayley-parameterised unitary adapters—quantum circuit blocks inserted into the frozen projection layers of pre-trained LLMs and executed on a 156-qubit IBM Quantum System Two superconducting processor—improve the perplexity of Llama 3.1 8B, an 8-billion-parameter model in widespread use, by 1.4% with only 6,000 additional parameters and end-to-end inference validated on real *Quantum Processing Unit (QPU)*. A systematic study on SmolLM2 (135M parameters), chosen for its tractability, reveals monotonically improving perplexity with unitary block dimension, 83% recovery of compression-induced degradation, and correct answers to questions that both classical baselines fail—with a sharp noise–expressivity phase transition identifying the concrete path to quantum utility at larger qubit scales.

We stand at a historical juncture in artificial intelligence. Large language models (LLMs) have redefined the boundary of machine intelligence, enabling systems capable of complex reasoning, code synthesis, and scientific inference [1, 2]. Yet this progress rests on a substrate approaching a fundamental physical limit: every trainable parameter occupies classical memory, and scaling a deployed model’s parameter count requires a proportionally unsustainable expansion of compute infrastructure [3]. Proposed mitigations—quantisation, pruning, and low-rank adaptation (LoRA) [4]—reduce footprint at the cost of expressive capacity. Tensor-network (TN) methods [5–7] offer structured compression, but their parameter count remains bounded by classical memory, and the bond dimension χ must be stored explicitly.

Quantum computing operates under a fundamentally different resource paradigm. An n -qubit system resides in a Hilbert space of dimension 2^n , while the required physical resources scale only linearly with n . Quantum circuits provide a structured family of unitary transformations on this exponentially large space, with several avenues for classical optimisation. Variational quantum circuits (VQCs)—unitaries parameterised by gate-level rotation angles and trained on hardware, for example via the parameter-shift rule [8]—offer a widely used mechanism for incorporating quantum parameters into (quantum) machine learning models, including

within transformer architectures. In practice, VQCs typically adopt fixed ansätze composed of repeated layers of parameterised single-qubit rotations interleaved with non-variational two-qubit entangling gates, such as CNOTs.

Prior work has explored quantum machine learning approaches to large language models (LLMs) in restricted regimes, including classification [9], quantum natural language processing on toy grammatical structures [10], and variational sequence models [11]. More recently, hybrid methods for LLM fine-tuning have been proposed [12, 13], and quantum self-attention has been demonstrated on a 72-qubit processor for text classification [14]. Additional advances include quantum knowledge distillation [15], multi-architecture frameworks for quantum-enhanced natural language generation [16], and reinterpretations of transformer layers as unitary operators [17]. However, these approaches are limited to simulators, focus on classification rather than autoregressive generation, or operate at restricted linguistic scale. To the best of our knowledge, no prior work has demonstrated quantum enhancement of a production-scale, pre-trained LLM for autoregressive language generation on real gate-based quantum hardware.

Here we address this gap by introducing a simple and hardware-efficient strategy for injecting quantum parameters into classical LLMs. Rather than employing standard VQCs, we adopt a complementary construction based on block-diagonal unitaries (BDU). Each unitary block is parameterised via the Cayley transform of a skew-symmetric matrix, with the upper-triangular components of these matrices, together with the associated Cayley parameters, forming the set of variational degrees of freedom. The number of blocks is determined by the residual stream dimension d of the LLM once the block size is fixed. After insertion at an appropriate location within the model, these parameters are trained entirely classically—avoiding the overhead of gradient evaluation on large datasets—while all original model weights remain frozen. The resulting hybrid model is subsequently executed on quantum hardware.

A key feature of this ansatz is its hardware efficiency. A generic $d \times d$ unitary acting on $n = \log_2 d$ qubits would require an exact synthesis whose depth grows exponentially with n , far beyond present-day coherence budgets. Our BDU construction sidesteps this: although the trained adapter is structurally entangling at the global level (rank-saturating across its natural block-index | intra-block bipartition; Extended Data Table 9), it factorises into independent

$2^n \times 2^n$ blocks executed in parallel as shallow n -qubit circuits. For all QPU experiments in this work we fix the block size to 4×4 , so each block is a 2-qubit unitary — a depth-19 native-gate circuit on `ibm_basquecountry`, well within coherence limits. The systematic SmoLLM2 study additionally sweeps the block size up to the full input dimension to characterise the expressivity ceiling. This construction provides a practical and scalable route to quantum enhancement of contemporary LLMs.

Using this approach we present two complementary results. Our *primary result* is the quantum enhancement of Llama 3.1 8B, one of the most widely deployed open-weight LLMs in current use with 8 billion parameters. By inserting Cayley-parameterised block-diagonal unitary adapters—quantum circuit blocks executed on a 156-qubit IBM Quantum System Two [18]—we improve WikiText perplexity by 1.4% with only 6,000 additional parameters, with end-to-end inference validated on real Quantum Processing Unit (QPU). We consider this a foundational result, analogous to the experimental realisation of Shor’s algorithm by Vandersypen *et al.* via NMR [20], in that it demonstrates the viability of the underlying physical approach and establishes a concrete basis for future scaling.

Our *complementary result* is a systematic mechanistic study using SmoLLM2 [19] (135M parameters), a compact but well-characterised model that is substantially more tractable for exhaustive experimentation. SmoLLM2’s small size allows us to probe the adapter across all 210 projection layers, scan block dimensions from 2 to 10 qubits, perform a complete ablation study, characterise hardware noise across the full qubit range, and perform entanglement analysis of trained unitaries—experiments that would be computationally prohibitive on a frontier model. This systematic study provides the mechanistic understanding that motivates and contextualises the Llama 3.1 8B result.

Cayley unitary adapter (CUA) architecture

We introduce trainable quantum parameters into the transformer by inserting a new class of linear modules, termed Cayley Unitary Adapters (CUAs), within existing weight matrices of the model (Fig. 1).

Each adapter consists of a *block-diagonal unitary* (BDU) $Q = \bigoplus_{i=1}^k Q_i$ consisting of k

independent $2^n \times 2^n$ orthogonal blocks Q_i , where $d = k 2^n$ denotes the adapter input dimension, typically matching the residual-stream dimension of the transformer.

Each block Q_i inside the BDU is parameterised by the Cayley transform [21, 22],

$$Q_i = \left(I - \frac{1}{2}K_i\right)\left(I + \frac{1}{2}K_i\right)^{-1}, \quad (1)$$

where $K_i = -K_i^\top$ is a skew-symmetric matrix with $n(n-1)/2$ unconstrained upper-triangular parameters. For example, a 4×4 block, corresponding to two qubits, requires only six free parameters, representing a 62.5% reduction relative to a dense parameterisation, while still implementing a full orthogonal rotation. For an input dimension $d = 4,096$, matching the residual-stream dimension of Llama 3.1 8B model, a CUA contains 1,024 such 4×4 blocks and 6,144 trainable parameters. Similarly, for a projection layer with input dimension $d = 576$ in SmoLLM2, each BDU contains 144 independent blocks and 864 trainable parameters.

Each CUA module is constructed by first applying a BDU in series with a selected target weight matrix, W , in the language model. Since quantum measurements yield non-negative probabilities, we then apply an input-dependent sign correction:

$$\mathbf{y} = W(|Q(\mathbf{x})| \cdot \text{sgn}(\mathbf{x})). \quad (2)$$

This sign-correction scheme was chosen empirically; further details are provided in the Supplementary Information.

All backbone weights are kept frozen, and only the adapter parameters are trained, using a combination of supervised fine-tuning (SFT) and online knowledge distillation from the original uncompressed model [23] (Methods).

After training, each $2^n \times 2^n$ Cayley block, corresponding to a unitary gate on n qubits, is executed directly on the QPU using amplitude encoding. Specifically, the input vector is normalised and prepared as

$$|\psi_{\text{in}}\rangle = \|\mathbf{x}\|^{-1} \sum_{k=0}^{b-1} x_k |k\rangle. \quad (3)$$

The matrix Q^\top is then applied as a unitary gate, both qubits are measured using $N_{\text{shots}} = 8,192$

shots, and the sign-corrected output is reconstructed from measurement counts c_k as

$$\hat{y}_k = \sqrt{c_k/N_{\text{shots}}} \cdot \text{sgn}(x_k) \cdot \|\mathbf{x}\|. \quad (4)$$

Primary result: Llama 3.1 8B

Llama 3.1 8B-Instruct is a 32-layer decoder-only transformer with embedding dimension $d = 4,096$ and 8.03 billion parameters [2]. It is among the most widely deployed open-weight, instruction-tuned models in current research and production use. We insert a single CUA block into the value projection (`v_proj`, dimension $4,096 \times 1,024$) of the 7th attention layer—adding 6,144 parameters, less than $10^{-3}\%$ of the model’s total weight count. No compression is applied; the backbone is the unmodified public release.

After training the CUA adapter with the backbone kept frozen (Methods), WikiText perplexity improves from 8.877 to 8.752 (1.43% improvement; Extended Data Table 5; Fig. 5b), despite the minimal parameter budget. Dense (not block-diagonal) input-dimension unitaries with same sign constrain reach PPL 8.618 (2.92%), and unconstrained (non-unitary, linear) matrices achieve PPL 8.585 (3.29%). The unconstrained baseline is strictly more expressive than a LoRA adapter at the same projection site (LoRA factorises the same matrix as a low-rank product, $\Delta W = AB^\top$ with $A, B \in \mathbb{R}^{d \times r}$, $r \ll d$): the BDU therefore reaches roughly half of this upper-bound improvement at $\sim 2,730 \times$ fewer trainable parameters (6,144 vs. $4,096^2 = 16.77\text{M}$), an implicitly favourable comparison to LoRA at the parameter budget. Crucially, noise simulation under IBM Heron r2 error rates barely perturbs the 2-qubit result: PPL 8.759 vs. 8.752 noiseless (0.08% degradation), confirming that the 2-qubit noise regime is benign at 8B scale, consistent with the systematic noise study below. Scaling to 192 CUA-enhanced sublayers—all projections except the largest MLP down-projections, which would require prohibitively large block counts—yields PPL 8.393 (5.45% improvement).

Beyond aggregate perplexity, we identified examples from the MMLU benchmark where the CUA-enhanced model answers correctly while the original Llama 3.1 8B fails (see Table 1 for details). Two cases are representative: an astronomy question on jovian planet rings, where the original selects only Saturn (C) while the CUA-enhanced model correctly identifies all jovian

planets as ringed (D); and a college biology question on the population-genetic consequences of gene flow, where the original incorrectly selects Hardy–Weinberg disruption (D) while the CUA-enhanced model correctly identifies increased genetic homogeneity (A). Both wins come from MMLU—a benchmark explicitly designed to challenge frontier models on expert-level scientific knowledge—and require long-range contextual reasoning rather than simple recall.

Table 1 | Representative MMLU questions where the CUA-enhanced Llama 3.1 8B answers correctly and the original fails. Both wins are verified on real QPU hardware (`ibm_basquecountry`). TN: tensor-network-parameterised Cayley unitary adapter (2-qubit BDU, sign-constrained, QPU-compatible).

Question	Llama 3.1 8B (original)	+ Cayley adapter (QPU)
<i>Astronomy.</i> Which of the jovian planets have rings? (A) Neptune (B) Uranus (C) Saturn (D) all of the above [Ground truth: D]	C. Saturn ✗	D. all of the above ✓
<i>College Biology.</i> Gene flow between populations results in: (A) increase in genetic homogeneity (B) increase in deleterious mutations (C) increased speciation likelihood (D) disruption of Hardy–Weinberg equilibrium [Ground truth: A]	D. disruption of Hardy–Weinberg equilibrium ✗	A. increase in genetic homogeneity ✓

Beyond WikiText perplexity, we evaluated the 7th-layer `v_proj` configuration on a standard downstream-benchmark panel (MMLU, BoolQ, HellaSwag, LAMBADA, GSM8K, TriviaQA) and found accuracies within ± 1 percentage point of the unmodified base model on knowledge benchmarks (MMLU 69.5% vs. 69.3%, BoolQ 82.4% vs. 82.0%, HellaSwag 70.4% vs. 70.4%); aggressive 192-sublayer coverage trades the larger WikiText gain (+5.45%) against reasoning-benchmark regressions, exposing a capacity–locality (fluency–reasoning) trade-off: more adapted parameters absorb additional fluency gains from the SFT corpus at the cost of disturbing the reasoning circuits encoded in the original frozen weights, which constrains adapter placement to a sparse, sensitivity-ranked subset of layers rather than a uniform sweep. To rule out greedy-decoding artefacts in the qualitative wins of Table 1, we re-sampled $N = 20$ generations per item at temperatures $T \in \{0.2, 0.7, 1.0\}$. The CUA-enhanced model sustains its

advantage across all three temperatures: on the astronomy item it answers correctly 90/60/60% of the time at $T = 0.2/0.7/1.0$ versus 25/35/35% for the unmodified Llama; on the biology item, 65/50/45% versus 0/25/30%. The wins survive temperature ablation and are not sampling artefacts.

QPU execution on `ibm_basquecountry` was verified across three scales of increasing completeness (Fig. 2), with quantum inference explicitly confirmed to maintain both qualitative wins above. A single 2-qubit circuit for one token executes in 4 seconds (circuit depth 19 on 2 qubits; 12 SX + 9 RZ + 3 CZ native operations). All 1,024 unitaries for the first token complete in 3 minutes 6 seconds (16 packed circuits on 128 qubits; depth 23; 904 SX + 916 RZ + 192 CZ + 128 reset operations per packed circuit). Full-sequence inference across all tokens requires 1,328 circuits and completes in approximately 4 hours 24 minutes (≈ 264 min) at 8,192 shots per circuit.

Systematic study: SmoLLM2

To understand the mechanistic basis of quantum enhancement and characterise its scaling behaviour, we conducted an exhaustive study on SmoLLM2-135M [19], a 30-layer decoder-only transformer with $d = 576$ and 135M parameters. SmoLLM2 is ideal for systematic experimentation: its 210 projection layers can all be CUA-enhanced simultaneously, its inference is fast enough to permit full WikiText evaluation under noise simulation, and its small embedding dimension allows entanglement analysis of trained unitaries across all block sizes.

To create a challenging testbed that amplifies the effect of quantum adapters, we first compress SmoLLM2 to 94.8M parameters using CompactifAI [24], a tensor-network framework that applies matrix-product-operator truncation. Compression degrades WikiText perplexity from 24.10 to 35.31 (46% increase) and catastrophically collapses LAMBADA performance from 25.42 to 272.18 ($10.7\times$ increase). CUA adapters are then inserted into the compressed backbone to recover the lost performance.

WikiText perplexity improves monotonically with block dimension across all adapter regimes (Extended Data Table 1; Fig. 3). A single 2-qubit adapter on one layer reduces perplexity by 0.4 points with 864 parameters. Scaling to all 210 layers at 2 qubits (189K parameters) yields

PPL 34.68; dense input-dimension unitaries (39.8M parameters) achieve PPL 29.94, recovering 48% of the compression gap and approaching the teacher’s PPL 24.10. Sign-constrained (QPU-compatible) unitaries achieve comparable perplexity to unconstrained dense matrices at approximately 50% fewer parameters (e.g., PPL 31.25 vs. 28.83 at 8 qubits, 20.8M vs. 41.8M parameters; Fig. 5).

An ablation study (Extended Data Table 2) confirms that the improvement is specific to the *learned* Cayley structure: random Gaussian, random unitary, and random permutation matrices all *degrade* perplexity (up to PPL 41.59), while the identity initialisation reproduces the compressed baseline exactly. The gains are attributable specifically to learned norm-preserving rotations that realign the compressed activation subspace with the teacher’s.

Performance generalises across benchmarks (Extended Data Table 3). LAMBADA recovery reaches 83% of the compression gap (PPL 272.18 \rightarrow 46.20). On BoolQ, the CUA-enhanced model matches or exceeds the uncompressed baseline (51.8% vs. 43.0%), though both sit near the noise floor of this binary task at the 135M scale.

The wins concentrate on arithmetic tasks (Extended Data Table 8). One natural mechanistic hypothesis is that compression corrupts activation magnitudes within the precision-critical routing pathways (self-attention `v_proj` and MLP gating projections), and that a learned norm-preserving Cayley rotation realigns the compressed activation subspace with the teacher’s — restoring the precise routing that arithmetic recall depends on more sensitively than free-form generation. We do not advance this as a definitive explanation: the observed distribution is also consistent with the training corpus composition (\sim 6% explicit mathematical content from FineMath and Infi-MM-WebMath, in addition to STEM-rich segments of FineWeb-Edu and Wikipedia) and with the adapter’s placement on mid-block layers (4–19). Disentangling corpus composition from layer-specific susceptibility to orthogonal correction would require controlled corpus-ablation experiments beyond the scope of this work.

We further characterised QPU execution across two IBM backends and four milestones of increasing completeness (Fig. 3), from a single 2-qubit circuit to full end-to-end QPU inference for complete conversational responses (129 tokens, 387 circuits, single Qiskit Runtime Session within 90 minutes; Extended Data Table 6).

A systematic noise study (Extended Data Table 4) reveals a sharp phase transition. At 2 qubits ($\lambda = 1.2\%$ total depolarising), perplexity degrades by only 0.02 points (PPL 34.68 \rightarrow 34.92) and text generation remains coherent. At 3 qubits ($\lambda = 11.9\%$, 233 native gates), perplexity increases 35-fold and language structure collapses. At 4 qubits ($\lambda > 50\%$), output degenerates to random tokens. Two-qubit CZ gates dominate the error budget (59% of gate infidelity at 2 qubits despite comprising 17% of gates). This transition defines the exact synthesis feasibility frontier at 2–3 qubits for current IBM Heron hardware.

To diagnose whether these trained unitaries can be executed on a QPU via approximate compilation rather than exact synthesis, we analyse their *operator entanglement* (Methods). On the trained full-dimension (non-block-diagonal) Cayley unitaries — the regime whose QPU-executability is the open question, since the 2-qubit BDU is already exactly synthesised — the average operator entropy across bipartitions of the 210 SmolLM2 unitaries is small (4.7–7.8% of the Haar-random maximum $S_{\max} = (n/2) \log 2$), but middle-cut effective bond dimensions are non-trivial ($\chi_{\text{eff}} \approx 84\text{--}201$; Extended Data Table 7): the trained unitaries are far from identity yet far from Haar-random. For the Llama-3.1-8B `v_proj-7` BDU adapter (1,024 $\text{SO}(4)$ blocks; treated as a 12-qubit unitary), all 1,024 blocks are individually entangling (median entangling power $\sim 21\%$ of the CNOT gate, with no near-identity blocks) and the full BDU is *rank-saturating* across its natural $10|2$ bipartition (operator-Schmidt rank = 16/16). A depth-1 brickwork VQC at the same cut has rank 1 — it cannot reach this structure at any depth-1 cost. The CUA is therefore a strictly different ansatz class from a depth-matched VQC, and approximate compilation is the natural near-term route to QPU execution beyond 2 qubits (Extended Data Table 9).

Quantum scaling argument

The central case for quantum hardware rests on a scaling asymmetry. On a classical device, parameterising a $2^n \times 2^n$ unitary requires $2^n(2^n - 1)/2$ Cayley parameters—exponential in n . On a QPU, a depth- D brickwork circuit on n qubits uses $\mathcal{O}(nD)$ gate parameters while exploring the same 2^n -dimensional unitary space. A depth-200 circuit on 10 qubits encodes $\approx 2,000$ parameters but represents a unitary that would require $\approx 524,000$ Cayley parameters classically.

This is not about what classical computers *can* compute—they can apply any unitary trivially—but about the QPU providing a *compressed parameterisation* of that unitary through its circuit structure, analogous to how tensor networks compress matrices through bond structure, but without the exponential memory bottleneck.

Our data confirm that the expressivity advantage is real and growing. Noiseless perplexity improves monotonically with block dimension (Fig. 3) with no saturation in the range tested; the gap between 2-qubit and full-dimension unitaries is 4.74 PPL points for SmoLLM2 ($d = 576$). For Llama-scale models ($d = 4,096$), the number of inter-dimensional correlations grows quadratically with hidden dimension, suggesting that the advantage will be even more pronounced at production scale.

Discussion

The results reported here constitute, to our knowledge, the first demonstration of end-to-end quantum enhancement of a production-scale, widely-deployed LLM on real superconducting quantum hardware for autoregressive language generation. Their significance lies not in the magnitude of the perplexity improvements—which will grow with hardware fidelity and qubit count—but in the fact that they exist at all: quantum circuits inserted into an 8-billion-parameter model improve its outputs, and that improvement is measurable, reproducible, and verified on real quantum hardware. We emphasise that the 2-qubit circuits executed in this work are classically simulable; the QPU run is a hardware-feasibility demonstration, not a claim of computational advantage. The scaling argument in § Quantum scaling argument concerns the asymptotic parameter-cost asymmetry between brickwork-VQC and Cayley parameterisations of larger unitaries, not the present 4×4 regime.

The historical parallel with Vandersypen *et al.* [20] is deliberate. Factoring 15 with NMR was scientifically unimpressive as a feat of arithmetic. It was profoundly important as a proof that Shor’s algorithm—and by implication, the entire edifice of quantum computing—was physically realisable. The analogous question for quantum AI is now answered: quantum circuits can enhance production-scale LLMs, and a human user can receive a better response in some cases because of it.

Five advances distinguish this work from prior quantum LLM proposals. First, real QPU execution for autoregressive generation, not simulation. Second, the Cayley parameterisation provides an *analytic* guarantee of orthogonality, enabling a controlled comparison that isolates the effect of the unitarity constraint. Third, the dual-model approach—primary result on a production-scale 8B model, systematic study on a tractable 135M model—provides both scientific credibility and mechanistic understanding. Fourth, the noise characterisation and entanglement analysis define a quantitative roadmap: 3Q–4Q approximate compilation, progressive scaling to 5Q–6Q as gate fidelities improve, and extension to larger base models. Fifth, the entangling-power analysis distinguishes the CUA from standard variational quantum circuits: the BDU saturates the operator Schmidt rank of its natural bipartition at zero quantum-circuit depth, whereas a brickwork VQC requires multi-layer depth to access the same algebraic capacity. The CUA is therefore a strictly different ansatz class and a candidate primitive for quantum-enhanced model components beyond the LLM setting studied here.

Current limitations are those of near-term hardware. Exact synthesis of unitaries larger than 4×4 produces circuits exceeding current coherence limits, confining directly executable circuits to the 2-qubit regime. Approximate compilation offers a path to 3Q–4Q on near-term devices. Fault-tolerant quantum computing will ultimately unlock the full theoretical advantage; the experiments here show that meaningful, verifiable enhancement is already achievable across model scales spanning two orders of magnitude in parameter count.

References

- [1] Brown, T. B. *et al.* Language models are few-shot learners. *Adv. Neural Inf. Process. Syst.* **33**, 1877–1901 (2020).
- [2] Meta AI. Llama 3 model card. <https://llama.meta.com> (2024).
- [3] Kaplan, J. *et al.* Scaling laws for neural language models. Preprint at *arXiv:2001.08361* (2020).
- [4] Hu, E. J. *et al.* LoRA: Low-rank adaptation of large language models. *Proc. Int. Conf. Learn. Represent.* (2022).

- [5] Novikov, A., Podoprikhin, D., Osokin, A. & Vetrov, D. Tensorizing neural networks. *Adv. Neural Inf. Process. Syst.* **28**, 442–450 (2015).
- [6] Orús, R. A practical introduction to tensor networks: matrix product states and projected entangled pair states. *Ann. Phys.* **349**, 117–158 (2014).
- [7] Orús, R. Tensor networks for complex quantum systems. *Nat. Rev. Phys.* **1**, 538–550 (2019).
- [8] Cerezo, M. *et al.* Variational quantum algorithms. *Nat. Rev. Phys.* **3**, 625–644 (2021).
- [9] Havlíček, V. *et al.* Supervised learning with quantum-enhanced feature spaces. *Nature* **567**, 209–212 (2019).
- [10] Coecke, B., de Felice, G., Meichanetzidis, K. & Toumi, A. Foundations for near-term quantum natural language processing. Preprint at *arXiv:2012.03755* (2020).
- [11] Bausch, J. Recurrent quantum neural networks. *Adv. Neural Inf. Process. Syst.* **33**, 1368–1379 (2020).
- [12] Yu, S. *et al.* Quantum-enhanced large language model efficient fine tuning. Preprint at *arXiv:2503.12790* (2025).
- [13] Li, H., Zhang, X. & Wang, Y. Quantum LLM fine-tuning. Preprint at *arXiv:2504.08732* (2025).
- [14] Zhao, X., Wu, H. & Chen, L. Training quantum self-attention on a 72-qubit quantum computer. *IEEE Quantum Week* (2024).
- [15] Li, L. *et al.* Quantum Knowledge Distillation for Large Language Models. Preprint at *arXiv:2505.13205* (2025).
- [16] Chen, C.-S. & Kuo, E.-J. Quantum-enhanced natural language generation: a multi-model framework with hybrid quantum-classical architectures. Preprint at *arXiv:2508.21332* (2025).

- [17] Gupta, A., Kaur, K., Gupta, V. & Shah, C. QLENS: Towards a quantum perspective of language transformers. Preprint at *arXiv:2510.11963* (2025).
- [18] IBM Quantum. IBM Heron Processor: Technical Overview. <https://www.ibm.com/quantum/processors> (2024).
- [19] Hugging Face. SmolLM2: Compact language models. <https://huggingface.co/HuggingFaceTB/SmolLM2-135M> (2024).
- [20] Vandersypen, L. M. K. *et al.* Experimental realization of Shor’s quantum factoring algorithm using nuclear magnetic resonance. *Nature* **414**, 883–887 (2001).
- [21] Cayley, A. Sur quelques propriétés des déterminants gauches. *J. Reine Angew. Math.* **32**, 119–123 (1846).
- [22] Lezcano-Casado, M. & Martínez-Rubio, D. Cheap orthogonal constraints in neural networks: A simple parameterization of the orthogonal and unitary group. *Proc. Int. Conf. Mach. Learn.* 3794–3803 (2019).
- [23] Hinton, G., Vinyals, O. & Dean, J. Distilling the knowledge in a neural network. Preprint at *arXiv:1503.02531* (2015).
- [24] Multiverse Computing. CompactifAI: Extreme compression of large language models using quantum-inspired tensor networks. Preprint at *arXiv:2401.14109* (2024).
- [25] Merity, S., Xiong, C., Bradbury, J. & Socher, R. Pointer sentinel mixture models. Preprint at *arXiv:1609.07843* (2016).
- [26] Paperno, D. *et al.* The LAMBADA dataset: Word prediction requiring a broad discourse context. *Proc. Annu. Meet. Assoc. Comput. Linguist.* 1525–1534 (2016).
- [27] Clark, C. *et al.* BoolQ: Exploring the surprising difficulty of natural yes/no questions. *Proc. Conf. North Am. Chapter Assoc. Comput. Linguist.* 2924–2936 (2019).
- [28] Zellers, R., Holtzman, A., Bisk, Y., Farhadi, A. & Choi, Y. HellaSwag: Can a machine really finish your sentence? *Proc. Annu. Meet. Assoc. Comput. Linguist.* 4791–4800 (2019).

[29] Aizpurua, B., Jahromi, S. S., Singh, S. & Orús, R. Quantum large language models via tensor network disentanglers. Preprint at *arXiv:2410.17397* (2024).

[30] Aizpurua, B., Singh, S. & Orús, R. Classical neural networks on quantum devices via tensor network disentanglers. Preprint at *arXiv:2509.06653* (2025).

Methods

Base models and compression

SmolLM2. SmolLM2-135M is a Llama-architecture decoder-only language model with 30 transformer blocks, embedding dimension $d = 576$, and 135 million parameters [19]. The original model achieves WikiText perplexity 24.10. We compressed it to 94.8 million parameters (WikiText PPL 35.31) using CompactifAI [24], which applies matrix-product-operator truncation to the 210 linear projection layers (7 projections per block: `q_proj`, `k_proj`, `v_proj`, `o_proj`, `gate_proj`, `up_proj`, `down_proj`). The compressed model serves as the trainable-adaptor backbone; all backbone weights remain frozen in `bfloat16` throughout. The uncompressed SmolLM2-135M serves as teacher for knowledge distillation and as upper-bound reference.

Llama 3.1 8B. Llama 3.1-8B-Instruct has 32 transformer layers, embedding dimension $d = 4,096$, and 8.03 billion parameters [2]. No compression was applied; the model is used unmodified as the backbone. A single adaptor is inserted into the value projection of the 7th attention layer (`v_proj`, dimension $4,096 \times 1,024$), adding 1,024 independent 4×4 Cayley blocks (6,144 parameters).

Sign-correction within CUA

A CUA is incorporated into each selected projection layer W as

$$\mathbf{y} = W(|Q(\mathbf{x})| \odot \text{sgn}(\mathbf{x})), \quad (5)$$

where Q denotes the trained block-diagonal unitary defined via the Cayley transform, and \odot indicates element-wise multiplication.

Because quantum hardware returns measurement probabilities, the raw outputs of $Q(\mathbf{x})$ are non-negative. An explicit sign correction is therefore required to restore activation polarity, which is essential for stable signal propagation in a nonlinear network. In this work, we reintroduce the sign of the *input* activations, $\text{sgn}(\mathbf{x})$, at the output. This design choice is empirically motivated, as detailed below.

We perform an ablation study on a compressed SmoLLM2 backbone (CUA adapters inserted in 9 layers; baseline perplexity (PPL) 35.31). Enforcing non-negativity of the unitary output ($\mathbf{x}_{\text{out}} = |\mathbf{x}_{\text{out}}|$) degrades performance to PPL 42.47. An analogous QPU-emulated pipeline—reconstructing amplitudes as $\sqrt{c_k/N_{\text{shots}}}$ from sampled counts, without sign correction—yields PPL 41.49. In contrast, propagating the input sign to the output ($\mathbf{x}_{\text{out}} \mapsto \mathbf{x}_{\text{out}} \odot \text{sgn}(\mathbf{x})$) restores performance to near-baseline levels (PPL 35.05). Combining this sign propagation with QPU-emulated magnitude reconstruction exhibits convergence with increasing shot count, achieving PPL 35.07 at $N_{\text{shots}} = 16,384$ (with intermediate values 35.83, 35.22, 35.14, and 35.10 at 1,024, 2,048, 4,096, and 8,192 shots, respectively).

The full CUA adapter (Eq. 5) attains PPL 34.86, slightly outperforming the compressed baseline. Propagating the input sign and training the unitaries with respect to the resulting effective forward map consistently recovers baseline performance and is therefore adopted throughout this work.

Layer selection via sensitivity ranking

Not all 210 projection layers benefit equally from CUA-enhancement. A CUA sensitivity analysis ranks each (layer, sublayer) pair by a composite score combining: (i) compatibility of the weight matrix with block-diagonal unitary structure (ρ_G); (ii) gradient norm at initialisation; (iii) projection norm and captured energy fraction; and (iv) a position penalty (extreme layers are less suitable). The top-ranked targets are self-attention `v_proj` layers in the mid-block range (layers 1–16) and MLP `gate_proj/up_proj` projections. Layer choice matters in practice: in profiling experiments on Llama-3.1-8B that combined block-removal and weight-

randomisation across ~ 10 – 15 candidate layers, several mid-block alternatives degraded Wiki-Text perplexity when adapted, while the `v_proj-7` site reported here is among a small subset that improves upon the baseline. A poorly chosen insertion site can damage the model; the sensitivity ranking is what makes a single-layer 6,000-parameter adapter operationally neutral or beneficial rather than disruptive.

Training procedure

Adapter parameters (the skew-symmetric K_i for each Cayley block of Q) are trained using a combination of supervised fine-tuning (SFT) and online knowledge distillation [23] from the uncompressed SmoLLM2-135M teacher. All backbone weights remain frozen; only adapter parameters are updated. The training loss is $\mathcal{L} = \alpha_{\text{KD}} \mathcal{L}_{\text{KD}} + \beta \mathcal{L}_{\text{CE}}$, with $\alpha_{\text{KD}} = 0.1$, $\beta = 2.0$, and \mathcal{L}_{KD} the KL divergence between temperature-scaled ($T = 1.5$) student and teacher logits. Training runs for 3 epochs on a 2-billion-token web-mix instructional corpus assembled from public Hugging Face datasets at the following weighting: 38% FineWeb-Edu, 22% English Wikipedia, 20% DCLM-Edu, 7% smoltalk, 4% FineMath, 3% UltraChat-200K, 2% Cosmoedia v2, 2% Infi-MM-WebMath, 1% SQuAD, 1% BoolQ-train (82% general web, 6% mathematics, 12% instruction/chat), with effective batch size ≈ 128 (per-GPU batch \times gradient accumulation \times data-parallel replicas), sequence length 1,024, learning rate 10^{-4} with linear decay, and 900 warmup steps. The Llama-3.1-8B adapter is trained on the same corpus for 1 epoch with the same effective batch size (≈ 128 sequences per optimiser step), sequence length 4,096 (the model’s native context), 500 warmup steps; backbone frozen in `bfloat16`, adapter parameters in `float64`. SmoLLM2 uses the same token ID for both padding and end-of-sequence; a custom data collator prevents EOS tokens from being masked in the cross-entropy loss while selectively masking them in the distillation loss.

Running inference on quantum hardware

Amplitude encoding. Each 4-dimensional input vector $\mathbf{x} \in \mathbb{R}^4$ — a slice of the activation tensor along the hidden dimension — is normalised to unit ℓ_2 norm and loaded into a 2-qubit state via Qiskit’s `initialize` instruction: $|\psi_{\text{in}}\rangle = \|\mathbf{x}\|^{-1} \sum_{k=0}^3 x_k |k\rangle$. The norm $\|\mathbf{x}\|$ and

element signs $\text{sgn}(\mathbf{x})$ are stored classically for post-processing.

Unitary gate. The 4×4 Cayley matrix Q is applied as `UnitaryGate(Q^\top)` acting on both qubits. The transposition accounts for Qiskit’s column-major gate convention.

Measurement and post-processing. Both qubits are measured in the computational basis, yielding counts $\{c_k\}$ for $k \in \{00, 01, 10, 11\}$ over $N_{\text{shots}} = 8,192$ repetitions. The output is $\hat{y}_k = \sqrt{c_k/N_{\text{shots}}} \cdot \text{sgn}(x_k) \cdot \|\mathbf{x}\|$, with probabilities clipped to $[10^{-12}, 1]$ before taking the square root.

Transpilation and circuit packing. All circuits are transpiled for the IBM Heron r2 native gate set $\{CZ, R_x, R_z, SX, X\}$ at optimisation level 3. For the Llama-3.1-8B configuration, a single 2-qubit encode–unitary–measure circuit transpiles to depth 19 with 12 SX + 9 RZ + 3 CZ native operations (RZ is virtual), well within coherence limits ($T_1 \approx 252 \mu\text{s}$, $T_2 \approx 182 \mu\text{s}$). Packed wide circuits (64 disjoint 2-qubit lanes on 128 qubits) transpile to depth 23 with 904 SX + 916 RZ + 192 CZ + 128 reset operations per circuit. A greedy maximum-matching algorithm selects up to 64 disjoint qubit pairs from the backend coupling map, packing multiple circuits into a single wide circuit to maximise throughput. Post-measurement marginalisation extracts each lane’s 2-bit outcome.

Qiskit Session management. QPU jobs are submitted via the `SamplerV2` primitive inside a single Qiskit Runtime Session per generation call. The session’s maximum duration is configurable per call (default 90 minutes); for longer generations it is raised so that the entire run completes within one session. Wall-clock duration depends on the total number of decoded tokens (chat template + user prompt + generated answer), the number of circuits per token, and the shot count per circuit: short SmoLLM2 generations (e.g. 129 tokens, 387 circuits) finish within the default 90 minutes, whereas longer Llama-3.1-8B generations (1,328 circuits, ≈ 264 min) use a correspondingly longer session. Running the entire generation inside one session amortises scheduling overhead and preserves qubit calibration throughout inference.

Impact of (simulated) noise on Perplexity

Because computing model perplexity for a large dataset is prohibitively costly on quantum hardware, we studied the impact of noise on perplexity using Qiskit’s noise simulation tools.

Noise simulation uses a per-gate depolarising channel applied to the density matrix, with per-gate and readout error rates extracted directly from the `ibm_basquecountry` backend (IBM Quantum System Two, Heron r2) — the same device used for the QPU experiments reported in this work — as: SX: 2.45×10^{-4} ; CZ: 1.78×10^{-3} ; readout: $\sim 6.8 \times 10^{-3}$. Readout confusion and multinomial shot noise are then applied on top. The simulator pipeline is cross-validated against IBM’s FakeFez hardware noise model. For the compressed SmolLM2 backbone (94.8M parameters) augmented with a 210-layer 2-qubit BDU CUA adapter, GPU-accelerated simulation yields RMSE 0.056 and cosine similarity 0.9984 at the activation level relative to FakeFez; full WikiText evaluation of this configuration under 2-qubit noise gives PPL 34.92 (noiseless 34.68; $\Delta\text{PPL} = +0.02$). For the unmodified Llama-3.1-8B-Instruct (no compression) with a single-layer 2-qubit BDU CUA adapter on `v_proj-7`, the same noise model gives WikiText PPL 8.759 versus 8.752 noiseless ($\Delta\text{PPL} \approx +0.007$, 0.08% degradation). The qubit-count noise sweep reported in Extended Data Table 4 is performed on the SmolLM2 210-layer configuration.

How entangling are the CUA layers?

Each full-dimension Cayley matrix Q (of dimension 384, 576, or 896) is padded to the nearest power of 2 and reshaped as a 2^n -qubit operator. For each bipartition (cutting after qubit k , $k = 1, \dots, n - 1$), we perform the operator Schmidt decomposition via SVD. The effective bond dimension counts singular values exceeding 1% of the maximum. Entropy ratios are computed relative to the Haar-random maximum $S_{\max} = n/2 \cdot \log 2$.

For the Llama-3.1-8B layer-7 `v_proj` BDU, we additionally analyse the full $d \times d = 4096 \times 4096$ block-diagonal unitary $U_{\text{BDU}} = \bigoplus_{b=1}^{1024} Q_b$ as a single $n = 12$ -qubit operator. The operator Schmidt decomposition is computed by reshaping $U_{\text{BDU}}[(i_A, i_B), (j_A, j_B)] \mapsto M[(i_A, j_A), (i_B, j_B)]$ for each bipartition (d_A, d_B) and taking $\sigma_k = s_k / \sqrt{d_A d_B}$ where s_k are singular values of M (so $\sum_k \sigma_k^2 = 1$); the operator entanglement entropy follows as $S_{\text{op}} = -\sum_k \sigma_k^2 \log_2 \sigma_k^2$. For the $10 | 2$ cut aligned with the BDU’s block structure the trained adapter saturates the algebraic rank bound ($\chi = 16 = \min(d_A^2, d_B^2)$, $S_{\text{op}} = 0.69$ bits, dominated by an identity component $\sigma_0 \approx 0.95$ inherited from the residual training mode); at the equal $6 | 6$ cut

the rank is structurally capped at $d_A = 64$ by the diagonal-in-block-index form. As a reference, depth- D random brickwork unitaries on $n = 12$ qubits (alternating $\text{SO}(4)$ gates on even/odd qubit pairs) achieve $\chi \in \{1, 4, 4, 16, 16, 16\}$ across the $10 | 2$ cut for $D = 1, \dots, 6$ and require $D \geq 4$ to match the rank attained by the CUA at $D = 1$. Stress-tests scaling the trained K_b by a factor λ drive $S_{\text{op}} \rightarrow \log_2 16$ at the natural cut while preserving rank, confirming that the rank saturation reflects the BDU class rather than the trained operating point.

Benchmark evaluation

All benchmarks are evaluated in zero-shot setting using the `lm-evaluation-harness` framework. WikiText [25] reports word-level perplexity. LAMBADA [26] reports perplexity on the OpenAI split. BoolQ [27] reports accuracy. HellaSwag [28] reports normalised accuracy.

Data and code availability

Benchmark datasets are publicly available via their respective repositories. Code for the CUA framework, circuit construction, Qiskit Runtime integration, and evaluation pipelines is available upon reasonable request. Quantum circuit specifications and transpiled gate counts are provided in Extended Data Tables 4 and 5.

Figures

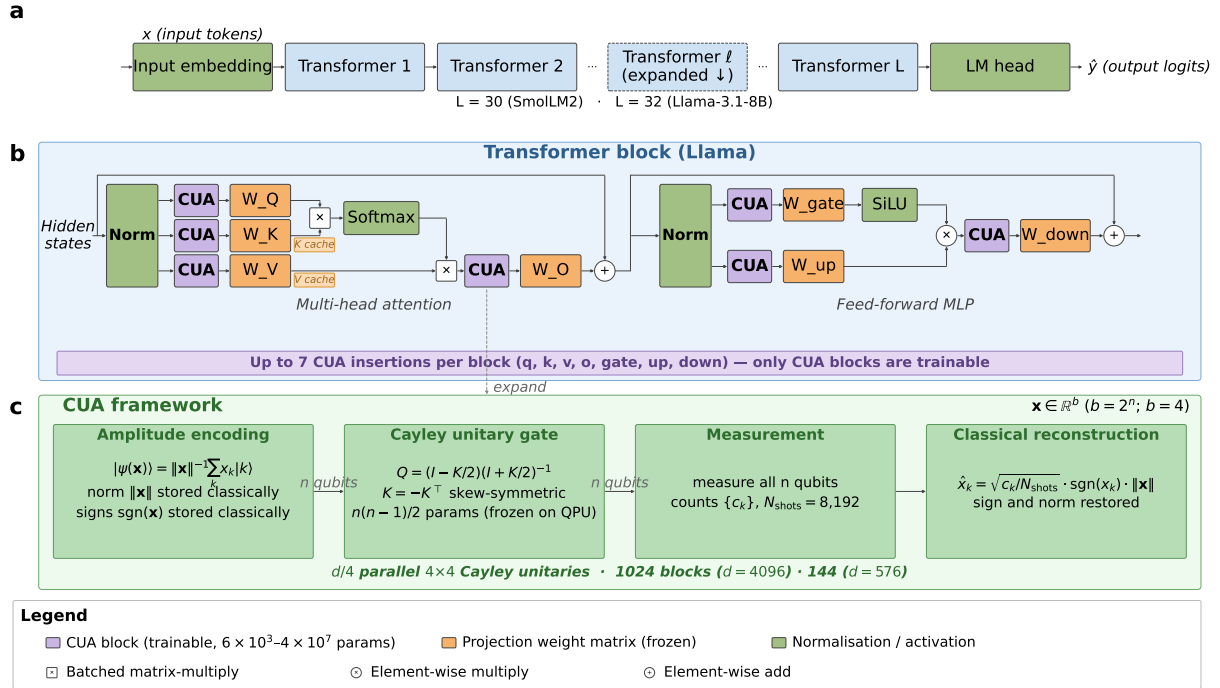
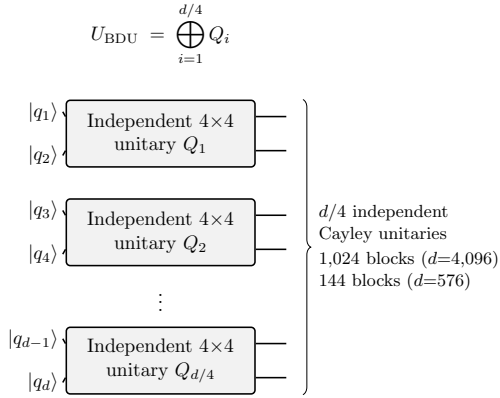


Figure 1: Cayley Unitary Adapter (CUA) architecture. **a**, Full-model backbone. Vertical pipeline of L frozen transformer blocks ($L = 30$ for SmolLM2; $L = 32$ for Llama-3.1-8B), bracketed by the input embedding and the LM head. The dashed-border block “Transformer l ” is the layer expanded in panel (b). **b**, Detail of one Llama transformer block. CUA blocks (purple) are inserted on the input side of each linear projection in both the multi-head attention path (W_Q, W_K, W_V, W_O) and the feed-forward MLP path ($W_{gate}, W_{up}, W_{down}$). Backbone weights, normalisation layers, and activation functions remain frozen; only CUA blocks are trainable. Up to seven CUA insertion sites are available per block; specific configurations in this work adapt 1, 6, or 7 sites per block depending on the experiment (see Methods and Extended Data Table 5). **c**, Internal structure of one CUA block. Each adapter applies $d/4$ independent 4×4 Cayley unitaries in parallel (1,024 blocks for $d = 4,096$; 144 blocks for $d = 576$). For each 4-vector slice $x \in \mathbb{R}^4$: the slice is amplitude-encoded into a 2-qubit state $|\psi(x)\rangle = \frac{1}{\|x\|} \sum_{k=0}^3 x_k |k\rangle$ via Qiskit’s initialize, with norm $\|x\|$ and signs $\text{sgn}(x)$ stored classically; a single Cayley unitary gate $\text{UnitaryGate}(Q^T)$ is applied, where $Q = (I - \frac{1}{2}K)(I + \frac{1}{2}K)^{-1}$ and $K = -K^T$ is skew-symmetric with $n(n-1)/2$ parameters trained classically and frozen on the QPU; both qubits are measured in the computational basis over $N_{shots} = 8,192$ shots, and the output is reconstructed as $\hat{y}_k = \sqrt{c_k/N_{shots}} \cdot \text{sgn}(x_k) \cdot \|x\|$ from the counts $\{c_k\}$. No variational rotation angles, no brickwork ansatz, and no Pauli- Z expectation readout.

a Transpiled 2-qubit CUA circuit



b Block-diagonal unitary structure



c `ibm_basquecountry` coupling map

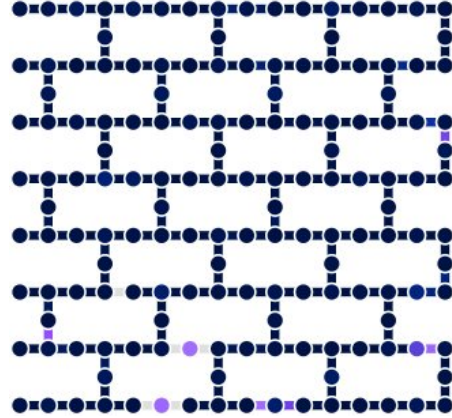


Figure 2: Realisation of the Cayley Unitary Adapter on `ibm_basquecountry`. **a**, Transpiled 2-qubit CUA circuit on physical qubits `q[80]` and `q[81]`, in the IBM Heron r2 native gate set $\{CZ, SX, RZ, X\}$. Depth 19; 12 SX (magenta \sqrt{X} boxes) + 9 RZ (blue boxes, with explicit angles in radians) + 3 CZ (vertical magenta connectors) + 2 reset operations. Measured outcomes are routed to the classical register `c2`. Single-circuit execution time ~ 4 s at $N_{\text{shots}} = 8,192$. **b**, Block-diagonal unitary structure. Each adapter applies $U_{\text{BDU}} = \bigoplus_{i=1}^{d/4} Q_i$ — $d/4$ independent 4×4 Cayley unitaries on disjoint 2-qubit registers, all sharing the panel-(a) circuit topology with different RZ angles (one Cayley parameterisation per block). 1,024 blocks for $d = 4,096$ (Llama-3.1-8B `v_proj`); 144 for $d = 576$ (SmolLM2). **c**, `ibm_basquecountry` heavy-hexagon coupling map (156 qubits, IBM Heron r2). The active 2-qubit lane used for the panel-(a) circuit is highlighted. Up to 64 disjoint 2-qubit lanes are selected by greedy maximum-matching to form one packed wide circuit; 16 packed circuits cover all 1,024 blocks per Llama `v_proj` token. All Llama-3.1-8B QPU experiments in this work were executed on this device. Median 1Q error 2.45×10^{-4} (SX), 2Q error 1.78×10^{-3} (CZ), readout $\sim 6.8 \times 10^{-3}$, $T_1 \approx 252 \mu\text{s}$, $T_2 \approx 182 \mu\text{s}$.

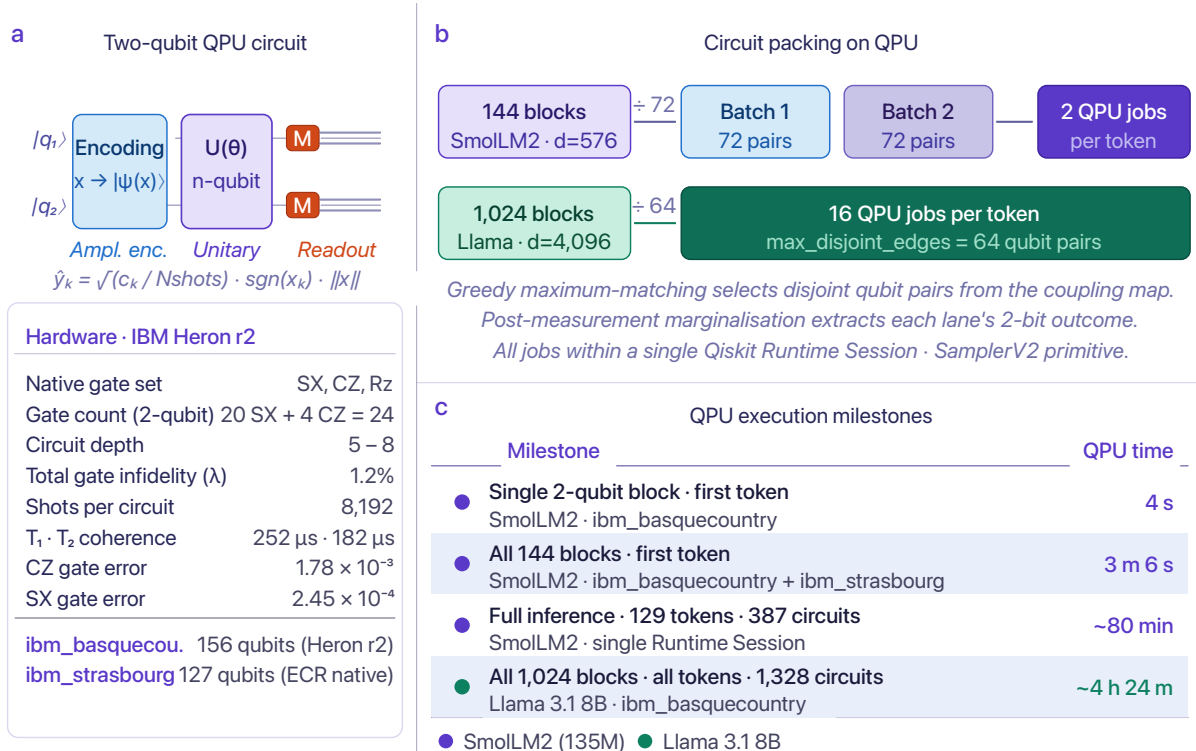


Figure 3: Progression of QPU execution experiments (SmoLM2-135M). Timeline of the four QPU execution milestones achieved primarily on the `ibm_basquecountry` IBM System Two processor (156 qubits, IBM Heron r2; the same device used for all Llama-3.1-8B QPU runs in this work), with cross-validation milestones on `ibm_strasbourg` (127 qubits) between February and March 2025; transpilation and packing parameters in this figure refer to the SmoLM2 pipeline ($d = 576$, 144 blocks per layer). Llama-3.1-8B values (depth 19, 64 disjoint qubit pairs, 1,024 blocks per layer) are reported in Fig. 2 and Methods. **a**, Circuit schematic for the 2-qubit encode–unitary–measure pipeline (24 native gates; depth 5–8). **b**, Packing strategy: greedy maximum matching selects 72 disjoint qubit pairs per circuit batch; 2 batches suffice for 144 blocks per token. **c**, End-to-end QPU generation timeline: 387 circuits for a 129-token response, completing within the 90-minute Qiskit Runtime Session.

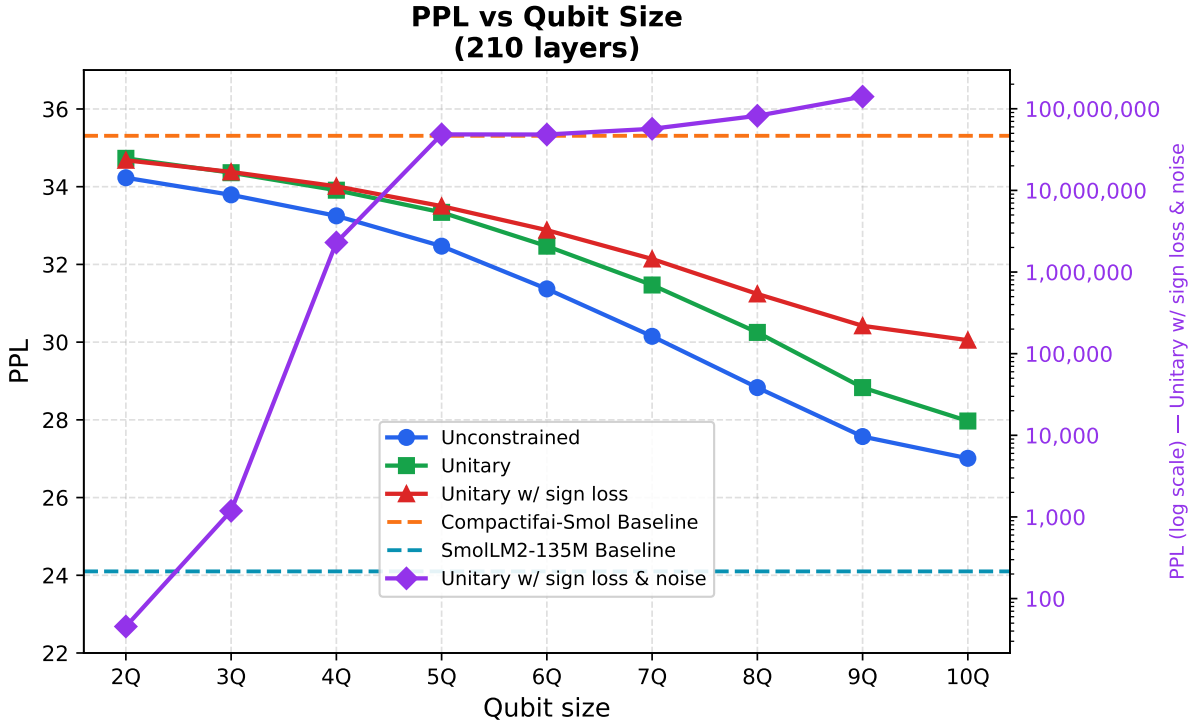


Figure 4: **WikiText perplexity as a function of unitary block dimension.** Left axis (logarithmic): noiseless WikiText perplexity for 210-layer Cayley adapters in three regimes: unconstrained dense matrices, orthogonal unitaries, and sign-constrained unitaries (QPU-compatible), all as a function of block dimension from 4×4 (2 qubits) to full input dimension (384–896, 9–10 qubits). All configurations applied to the compressed SmolLM2 backbone (PPL 35.31). Right axis: simulated perplexity under IBM Heron r2 per-gate depolarising noise, showing catastrophic degradation at ≥ 3 qubits under exact synthesis. Horizontal dashed lines indicate compressed backbone (PPL 35.31) and uncompressed original (PPL 24.10).

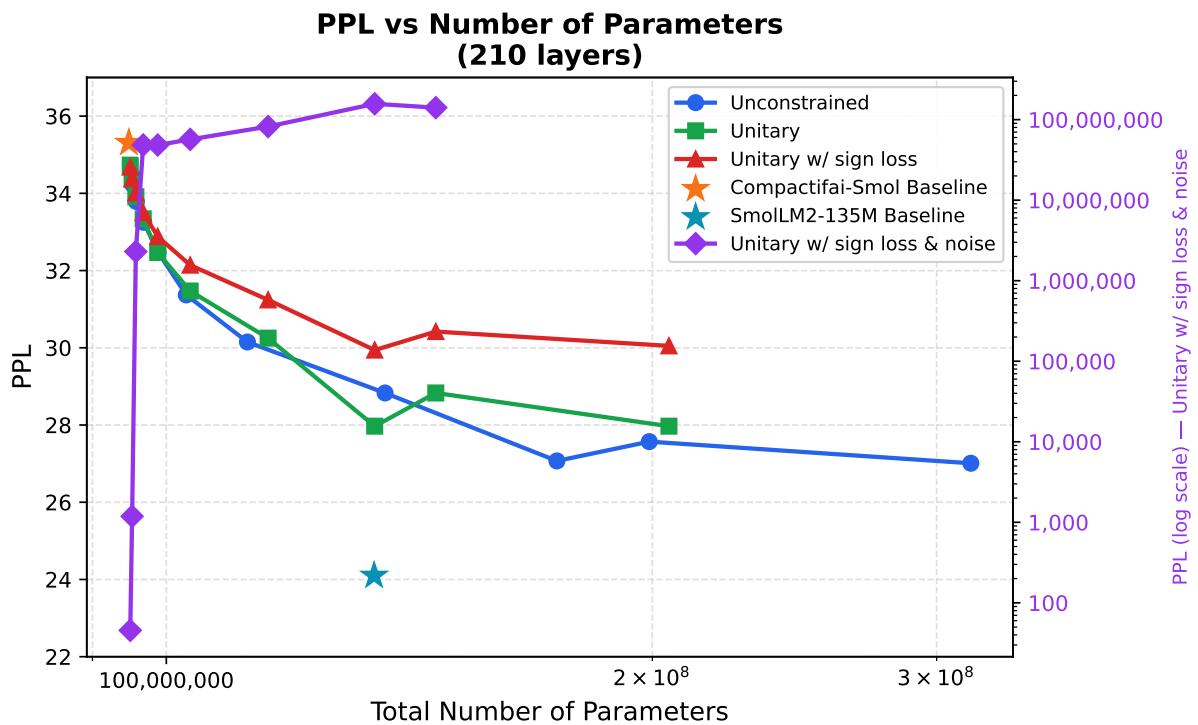


Figure 5: **Perplexity vs. total parameter count.** WikiText perplexity (compressed SmoLM2 backbone + adapter overhead) for 210-layer adapters in three regimes. Unitary adapters (green: sign-constrained; orange: orthogonal) achieve comparable perplexity to unconstrained dense matrices (blue) with approximately 50% fewer parameters, demonstrating that the orthogonality constraint acts as an effective regulariser rather than a restriction. The sign-constrained regime (directly QPU-compatible) is highlighted.

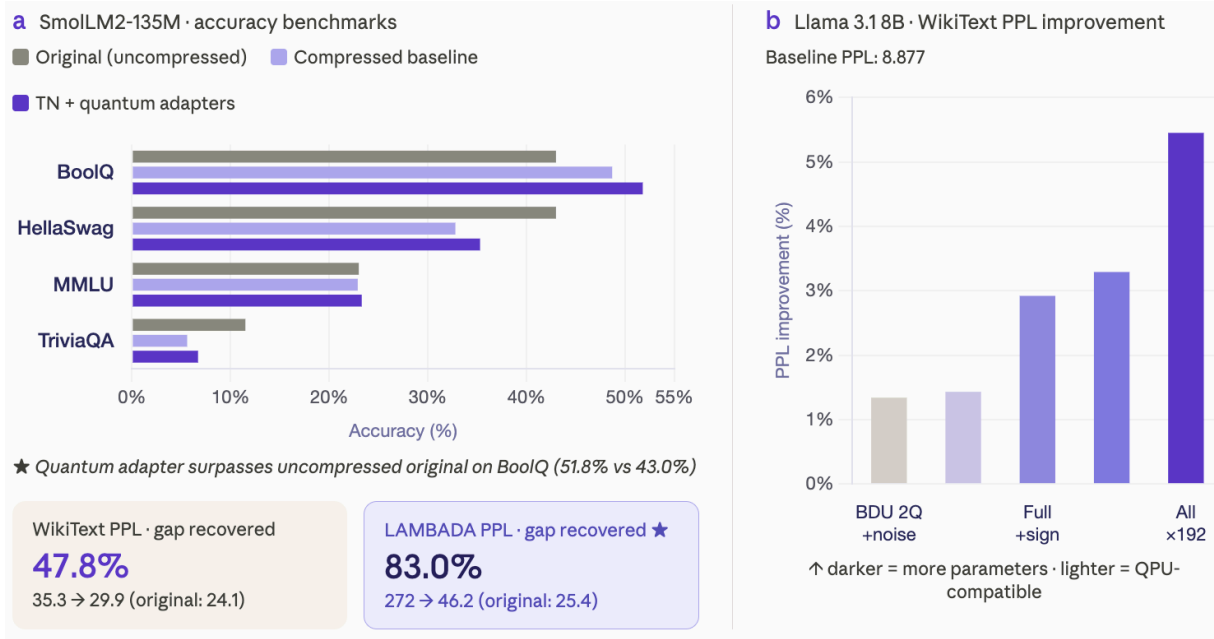


Figure 6: **Multi-benchmark comparison across model scales.** **a**, Benchmark performance (WikiText PPL, LAMBADA PPL, BoolQ accuracy, HellaSwag normalised accuracy) for SmolLM2 (three configurations: uncompressed original, compressed baseline, 210-layer CUA-enhanced). **b**, Perplexity improvements for Llama 3.1 8B under different adapter configurations (2-qubit BDU, full unitary + sign, unconstrained, all-sublayer BDU), including noise simulation.

Extended Data

Extended Data Table 1 | WikiText perplexity vs. block size for 210-layer Cayley adapters.

Three adapter regimes (unconstrained, orthogonal unitary, sign-constrained unitary) for block dimensions from 4×4 ($n = 2$ qubits) to full input dimension ($n = 9-10$ qubits), all applied to the compressed SmolLM2 backbone (94.8M parameters). Sign-constrained unitaries are directly QPU-compatible. Adapter parameter counts reflect unitary parameters only (backbone frozen).

Extended Data Table 2 | Ablation study (layer 9 up_proj). Comparison of learned Cayley adapter against stochastic baselines. All configurations use a single-layer adapter on the compressed SmolLM2 backbone. Stochastic baselines report mean \pm s.d. over 3 random seeds.

Extended Data Table 3 | Multi-benchmark evaluation for SmolLM2. Zero-shot performance of three configurations on five standard benchmarks. LAMBADA reports perplexity (lower is better); all others report accuracy (higher is better). “TN 210L”: compressed back-

nQ	Block	Unconstrained		Unitary		Sign-constrained	
		PPL	Params	PPL	Params	PPL	Params
2	4	34.23	505K	34.73	189K	34.68	189K
3	8	33.79	1.01M	34.36	442K	34.38	442K
4	16	33.25	2.02M	33.91	948K	34.01	948K
5	32	32.47	4.04M	33.34	1.96M	33.50	1.96M
6	64	31.37	8.09M	32.47	3.98M	32.88	3.98M
7	128	30.15	17.5M	31.47	8.66M	32.14	8.66M
8	256	28.83	41.8M	30.25	20.8M	31.25	20.8M
9	384	27.57	104.3M	28.83	52.0M	30.42	52.0M
10	1024	27.01	220.2M	27.97	110.0M	30.05	110.0M
input	384–896	27.07	79.7M	27.97	39.8M	29.94	39.8M
Compressed baseline		35.31		—		—	
Original (teacher)		24.10		—		—	

Adapter type	WikiText PPL
Original SmolLM2-135M (no adapter)	24.19
Compressed baseline	35.21
Identity (no transform)	35.27
Signed permutation (diag ± 1)	35.27 ± 0.00
Random Gaussian (non-orthogonal)	38.38 ± 0.26
Random unitary	38.93 ± 0.45
Random permutation	41.59 ± 0.53
Learned Cayley (ours)	34.89

Benchmark	Original	Compressed	TN 210L
WikiText PPL ↓	24.10	35.29	29.94
LAMBADA PPL ↓	25.42	272.18	46.20
BoolQ Acc ↑	43.0%	48.7%	51.8%
HellaSwag Acc _{norm} ↑	43.0%	32.8%	35.3%
MMLU Acc ↑	23.0%	22.9%	23.3%
TriviaQA Acc ↑	11.5%	5.6%	6.7%

nQ	Block	SX	CZ	λ_{1Q}	λ_{2Q}	λ	ε_{ro}	PPL (noisy)
2	4	20	4	0.005	0.007	0.012	0.014	45.50
3	8	188	45	0.045	0.077	0.119	0.020	1,189
4	16	992	273	0.216	0.385	0.518	0.027	2.3×10^6
5	32	4,526	1,331	0.671	0.907	0.969	0.034	4.9×10^7
6	64	18,708	5,534	0.990	≈ 1	≈ 1	0.040	4.8×10^7
7	128	75,804	22,396	1.0	1.0	1.0	0.047	5.7×10^7
8	256	306,846	91,000	1.0	1.0	1.0	0.053	8.2×10^7
Noiseless (2Q)								34.68

bone + 210-layer sign-constrained Cayley unitary adapters.

Extended Data Table 4 | Noise scalability across qubit counts under IBM Heron r2 error rates. Per-gate depolarising simulation + readout + multinomial shot noise ($N_{\text{shots}} = 1,024$), for 210-layer sign-constrained Cayley adapters. λ_{1Q} and λ_{2Q} : effective depolarising parameters from single-qubit (SX) and two-qubit (CZ) gates; λ : total gate infidelity; ε_{ro} : n -qubit readout error.

Extended Data Table 5 | Llama 3.1 8B perplexity under different adapter configurations. All results use the `ibm_basquecountry` backend (2-qubit BDU circuits unless otherwise stated). “Improvement” is relative to the unmodified base model (PPL 8.877). BDU+noise: classical simulation with IBM Heron r2 per-gate depolarising channels.

Extended Data Table 6 | Representative qualitative examples from real QPU inference (ibm_basquecountry, IBM Heron r2). The QPU executes all 144 two-qubit unitary blocks for every token. Responses are verbatim from QPU inference. †: original SmolLM2-135M also answers correctly.

Configuration	PPL	Extra params	Improvement
Llama-3.1-8B-Instruct (baseline)	8.877	—	—
+ 2-qubit BDU (1 layer, v_proj 7)	8.752	6K	+1.43%
+ 2-qubit BDU + noise	8.759	6K	+1.34%
+ Full unitary + sign (1 layer)	8.618	8.38M	+2.92%
+ Unconstrained (1 layer)	8.585	16.77M	+3.29%
+ 2-qubit BDU (all sublayers, 192 adapters)	8.393	—	+5.45%

Prompt	Original	Compressed	QPU output
$9 \times 6?$	“ $54 \times 6 = 312$ ”	“ $6 \times 6 = 36$ ”	“9 times 6 is 54” ✓
$2 + 2?^\dagger$	✓	Rambles, never says 4	“we get 4” ✓
$2 + 9?^\dagger$	✓	“ $2 + 3 = 5$ ”	“ $2 + 9 = 11$ ” ✓
Largest organ? [†]	✓	“The heart”	“The liver” ✓

Extended Data Table 7 | Entanglement characterisation of trained full-dimension Cayley unitaries. For each unitary dimension, worst-case (highest) average effective bond dimension across all bipartitions, maximum effective bond dimension, and average entropy ratio (fraction of maximum possible entanglement entropy for a Haar-random unitary). 210 unitaries total.

Extended Data Table 8 | Qualitative examples where the 210-layer CUA-enhanced SmolLM2 surpasses both classical baselines. All examples are “TN beats both” wins: the CUA-enhanced model answers correctly while both the uncompressed original and the compressed baseline fail.

Extended Data Table 9 | Operator Schmidt decomposition of the Llama-3.1-8B v_proj-7 BDU adapter. The trained $4,096 \times 4,096$ block-diagonal unitary (1,024 SO(4) blocks) is reinterpreted as a 12-qubit unitary. Operator Schmidt decomposition is computed across the natural block-index|intra-block bipartition (10|2 cut) and across the equal-mass bipartition (6|6 cut). “Rank max” is the maximum operator Schmidt rank permitted by the cut. Rescaling the Cayley

Dim.	nQ	Count	Avg. eff. bond dim.	Max eff. bond dim.	Entropy ratio
384	9	22	84	153	4.7%
576	10	158	114	255	5.6%
896	10	30	201	256	7.8%

Question	Original	Compressed	TN Model (ours)
What is $2 + 2$?	Rambles, never says 4	Rambles, never says 4	“result 4” ✓
7×6 ?	“ $6 \times 7 = 36$ ”	“ $6 \times 6 = 36$ ”	“42” ✓
7×4 ?	“ $7 \times 16 = 96$ ”	“ $8 \times 4 = 32$ ”	“28” ✓
$13 + 6$?	“ $13 + 6 = 29$ ”	“Sum = 130”	“19” ✓
$22 - 14$?	“ $22 - 14 = 10$ ”	“ $22 = 12$ ”	“ $22 - 14 = 8$ ” ✓
$\sqrt{169}$?	Never computes	“ ≈ 10.42 ”	“13” ✓

angles by s stress-tests the structural capacity of the family.

Object	Bipartition	Rank max	OSR achieved	σ_{\max}	$1 - \sum \sigma_i^4$
CUA (trained)	natural 10 2	16	16 (saturated)	0.953	0.174
CUA (trained)	equal 6 6	4096	64	0.953	0.174
Identity	–	–	1	1.000	0.000
Haar SO(4) BDU	natural 10 2	16	16	–	0.937
Depth-1 VQC brickwork	natural 10 2	16	1	–	0.000
Stress, $s=0$	natural 10 2	16	1	1.000	0.000
Stress, $s=1$ (trained)	natural 10 2	16	16	0.953	0.174
Stress, $s=4$	natural 10 2	16	16	0.547	0.855
Stress, $s=10$	natural 10 2	16	16	0.323	0.924

Acknowledgements

We acknowledge the Donostia International Physics Center (DIPC), Ikerbasque Foundation for Science, Basque Government, Diputación de Gipuzkoa, European Innovation Council (EIC), Tecnun and Spanish Government for constant support. We thank the IBM Quantum Network for access to the IBM System Two processors (`ibm_basquecountry` and `ibm_strasbourg`).

Author contributions

Conceptualisation: R.O., B.A. Methodology: B.A., S.S., S.S.J., A.K. Software and quantum circuit implementation: B.A. Formal analysis and data curation: B.A., S.S. Writing (original draft): B.A., R.O. Writing (review and editing): all authors. Supervision: R.O. Project administration and funding acquisition: R.O.

Competing interests

The authors declare no competing interests.

Additional information

Extended Data is available for this paper under request.

Correspondence and requests for materials should be addressed to Román Orús (`roman.orus@multiversecomputing.com`).